



Identification and Verification of a Novel Disulfidptosis-Related lncRNAs Prognostic Signature to Predict the Prognosis and Immune Activity of Head and Neck Squamous Carcinoma

Zi Yin ^{1,2}, Jue Wang ², Changqing Zhu ^{1,3}, Chenli Xu ^{1,4}, Juan Fang ^{1,2}, *Qiaoqin Li ^{1,2}

1. Department of Pathology, School of Basic Medicine, Hubei University of Medicine, Shiyan, China
2. Clinical Pathology Test and Consultation Center, Hubei University of Medicine, Shiyan, China
3. Department of Pathology, Shiyan Renmin Hospital, Hubei University of Medicine, Shiyan, China
4. Forensic Judicial Appraisal Institute, Hubei University of Medicine, Shiyan, China

*Corresponding Author: Email: darkingyz@163.com

(Received 20 Jan 2024; accepted 14 Apr 2024)

Abstract

Background: We aimed to explore the prediction value of disulfidptosis-related long noncoding RNAs (lncRNAs) on the prognosis and immunotherapy efficiency of patients with head and neck squamous carcinoma (HNSCC).

Methods: Clinical and RNA-seq information were collected from The Cancer Genome Atlas (TCGA) and Genome Data Sharing (GDC) portal. The Pearson correlation analysis, univariate COX regression analysis, the least absolute shrinkage and selection operator (LASSO) COX regression were employed to construct the disulfidptosis-related lncRNAs (DRLs) prognostic model. The Kaplan-Meier survival curve, principal component analysis (PCA), receiver operating characteristic (ROC) curves and areas under the curves (AUCs) were used to examine the accuracy of the prognostic model. ssGSEA, mutation and functional and gene set enrichment analysis was performed to quantify the immune cell infiltration, immune function and functional enrichments. Finally, the mRNA expression of the DRLs was verified by real-time PCR (RT-PCR) in HNSCC cells.

Results: A new DRLs prognostic model (*AC083967.1*, *AC106820.5*, *AC245041.2*, *AL590617.2*, *AP002478.1*, and *VPS9D1-AS1*) with an independent prognostic value of HNSCC patients was successfully identified. In addition, the DRLs prognostic model was related with immune signature and drug therapy response. Meanwhile, the mRNA expression level of the 6 DRLs detected by RT-PCR was consistent with the results of bioinformatic analysis.

Conclusion: We developed a new DRLs prognostic model of HNSCC, which could effectively predicate the prognosis and therapy response of HNSCC patients and provide insights into personalized therapeutics.

Keywords: Head and neck squamous carcinoma; Disulfidptosis; Long non-coding RNAs; Immune activity

Introduction

Head and neck squamous cell carcinoma (HNSCC) is the most common malignant tumor

in the world, with over 660000 new cases and 320000 deaths in 2020. The incidence rate of



Copyright © 2024 Yin et al. Published by Tehran University of Medical Sciences.
This work is licensed under a Creative Commons Attribution-NonCommercial 4.0 International license.
(<https://creativecommons.org/licenses/by-nc/4.0/>). Non-commercial uses of the work are permitted, provided the original work is properly cited

HNSCC ranks sixth and is rising and is estimated to increase by 30% by 2030 (1, 2). Over the past decades, the survival of HNSCC patients has improved adequately as a result of the progression in multimodality treatments. While the prognosis of HNSCC patients is still poor, and epidemiological data shows that the 5-year overall survival (OS) of HNSCC patients is approximately 60% (3). Therefore, its urge to explore the new prognostic model to achieve accurate and effective treatment methods and finally improve the survival of HNSCC patients.

Recently, Liu et al (4), reported the existence of a novel cell death type caused by disulfide stress, termed as disulfidptosis. The occurrence mechanism of disulfidptosis is still in its beginning stage. The reported disulfidptosis related genes (DRGs) ranges from 9 to 78 (5-8). Meanwhile, study showed the occurrence of disulfidptosis depends on the high expression level of Xc⁻ transporter consists of a light-chain subunit xCT (*SLC7A11*) as well as the tumor cells undergo glucose starvation (4). Interestingly, *SLC7A11* was overexpressed in HNSCC (9). Moreover, glucose was the dominate energy source of HNSCC proliferation and survival (10). Disulfidptosis is a new promising therapeutic target for the treatment of HNSCC, which deserves further exploration. However, there have been still no studies on the correlation of disulfidptosis and HNSCC.

Long non-coding RNA (lncRNA) is a kind of gene transcripts with length between 200 and 1000 nucleotides. Encoded by the genome but don't encode protein, lncRNAs are involved in the regulation of a variety of biological processes (11). Noticeably, lncRNAs play a vital role in the progression of HNSCC, including growth, metastasis, recurrence, drug resistant and other behaviors. For instance, *lncMX1-21* was induced by IFN α to negatively regulates immunosuppression of HNSCC cells by interrupting H3K27 acetylation (12). HNSCC patients with overexpressed *LINC02195* achieved a better outcome via enhancing the expression levels of MHC I mole-

cules (13). Meanwhile, disulfidptosis-related lncRNAs (DRLs) prognostic signatures could predict the survival outcomes for cancers (5-7). Exploring the DRLs signature would be another prognostic candidate for HNSCC, expected to be of great significance in promoting the overall survival of HNSCC patients.

The immune regulation determines the development of tumors and modulates the effect of immunotherapy (14). The investigation of the infiltration of immune cells in the tumor microenvironment (TME) is important for understanding the tumor progression. Noticeably, it has been reported that lncRNAs plays an immune regulation role in HNSCC (12, 13). While there are still a large number of lncRNAs related to immune regulation that have not been explored thoroughly. The delineation of the immunological role of DRLs in HNSCC maybe further provide new insights into the mechanism of the progression of HNSCC and consequently facilitate the more effective prognostic prediction and immunotherapy of HNSCC patients.

In the present study, we constructed a 6 DRLs prognostic model of HNSCC using a series of bioinformatics analysis. The accuracy of this prognostic model was confirmed and the immunotherapy response was analyzed.

Materials and Methods

Data collection

The HNSCC dataset including RNA sequencing (RNA-seq) and patients' clinical information were downloaded from The Cancer Genome Atlas (TCGA) database (<https://portal.gdc.cancer.gov/>). Removed data with missing survival status, unknown survival time, or survival < 30 d. Therefore, 511 patients with HNSCC and 44 healthy individuals were included in subsequent analyses. Last accessed of TCGA: Aug 2023 and the patient details were shown in Table 1. Overall, 23 DRGs were obtained from previous study (4) (Fig. 1).

Table 1: Clinicopathologic features of HNSCC patients

| Features | Type | Total N(%) | Test N(%) | Train N(%) | P-value |
|----------|-----------|---------------|--------------|---------------|---------|
| Age(yr) | <=65 | 338(66.14) | 170(66.67) | 168(65.62) | 0.8766 |
| | >65 | 173(33.86) | 85(33.33) | 88(34.38) | |
| Gender | Female | 133(26.03) | 67(26.27) | 66(25.78) | 0.9791 |
| | Male | 378(73.97) | 188(73.73) | 190(74.22) | |
| Grade | G1 | 61(11.94) | 37(14.51) | 24(9.38) | 0.2683 |
| | G2 | 298(58.32) | 151(59.22) | 147(57.42) | |
| | G3 | 123(24.07) | 60(23.53) | 63(24.61) | |
| | G4 | 7(1.37) | 2(0.78) | 5(1.95) | |
| | Unknown | 22(4.31) | 5(1.96) | 17(6.64) | |
| Stage | Stage I | 27(5.28) | 13(5.1) | 14(5.47) | 0.9094 |
| | Stage II | 70(13.7) | 35(13.73) | 35(13.67) | |
| | Stage III | 81(15.85) | 36(14.12) | 45(17.58) | |
| | Stage IV | 258(50.49) | 125(49.02) | 133(51.95) | |
| | Unknown | 75(14.68) | 46(18.04) | 29(11.33) | |
| T | T0 | 1(0.2) | 1(0.39) | 0(0) | 0.6958 |
| | T1 | 47(9.2) | 24(9.41) | 23(8.98) | |
| | T2 | 133(26.03) | 62(24.31) | 71(27.73) | |
| | T3 | 99(19.37) | 53(20.78) | 46(17.97) | |
| | T4 | 169(33.07) | 82(32.16) | 87(33.98) | |
| M | Unknown | 62(12.13) | 33(12.94) | 29(11.33) | 0.9912 |
| | M0 | 181(35.42) | 92(36.08) | 89(34.77) | |
| | M1 | 1(0.2) | 0(0) | 1(0.39) | |
| N | Unknown | 329(64.38) | 163(63.92) | 166(64.84) | 0.2259 |
| | N0 | 172(33.66) | 89(34.9) | 83(32.42) | |
| | N1 | 67(13.11) | 25(9.8) | 42(16.41) | |
| | N2 | 164(32.09) | 83(32.55) | 81(31.64) | |
| | N3 | 8(1.57) | 4(1.57) | 4(1.56) | |
| | Unknown | 100(19.57) | 54(21.18) | 46(17.97) | |

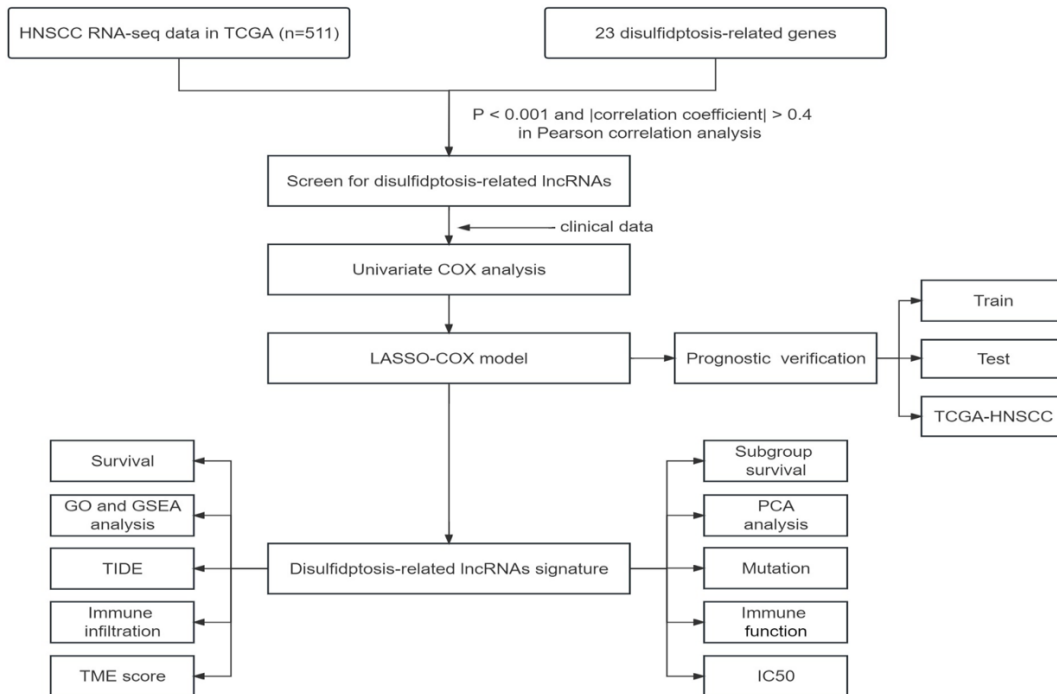


Fig. 1: Study design flowchart

Construction and verification of the DRLs prognostic model

The expression of 23 DRGs were extracted (Table S1- not published), and the co-expressed DRLs were obtained through Pearson correlation analysis. The screening criteria were $P < 0.001$ and $|\text{correlation coefficient}| > 0.4$. Before establishing the model, the DRLs were tested by univariate COX regression analysis ($P < 0.05$). HNSCC patients from TCGA database were randomly divided into training group and testing group. Then, in order to reduce the risk of overfitting and construct the prognostic model with optimal number of lncRNAs, LASSO COX regression was performed for the prognostic models and the risk score as follow:

$$\text{risk score} = \sum_{i=1}^n \text{coef}(i) * \text{expr}(i)$$

Coef represents the risk regression coefficient of DRLs, and X represents the DRLs expression levels. The risk score of each HNSCC patient was measured, and patients in training group and test group were divided into high- and low-risk groups according to the median risk score of training group, respectively. PCA analysis was performed to examine the accuracy of the prognosis model. Immediately afterward, Kaplan-Meier survival curve was conducted to explore whether the high-risk group has shorter overall survival (OS) than the low-risk group. The 1-, 3-, and 5-year survival ROC curves and multifactor ROC curve were used to assess the accuracy of model.

Tumor immune dysfunction and exclusion (TIDE) and prediction of drug therapy response analysis

The TIDE score of HNSCC patients was calculated using the online tool available at <http://tide.dfci.harvard.edu/>, and results were visualized using a violin plot. The “oncoRredict” and “parallel” packages were used to predict sen-

sitivity to antitumor drug therapy in both groups of patients.

Evaluation of immune cell infiltration

The relative percentage of each type of immune cell and the immune function score were calculated using the “limma”, “GSVA”, “GSEABase”, “ggpubr”, and “reshape2” packages. Stromal Score, Immune Score, and ESTIMATE Score were calculated using the “estimate” package, and the score of the tumor microenvironment were then compared between the two groups.

Mutation analysis

To identify the genes with the most significant mutation rates for further investigation, we used “maftools” package to construct mutation charts for high- and low-risk groups. And waterfall plots compared mutation profiles in high- and low-risk groups.

Functional and gene set enrichment analysis (GSEA)

False discovery rate (FDR) < 0.05 and $|\log_2 \text{fold change} (\text{fold change})| \geq 1$ were used as the criterion to screen differential genes in high- and low-risk groups. We then applied the “limma” and “clusterProfiler” packages to perform Gene Ontology (GO) analysis. Signaling pathway enrichment analysis was performed through GSEA, and enrichment maps were drawn using GSEA (4.1.1) software.

Real-time PCR

Total RNA was extracted using Trizol (Beyotime, Shanghai, China) and reverse transcribed into cDNA using a Prime Script™ RT Kit. Then the cDNA was subsequently amplified by real-time PCR (RT-PCR) using SYBR Green qPCR Master Mix (ABclonal, Beijing, China). GAPDH was used as the internal reference and the relative expression of mRNA was calculated by the $2^{-\Delta\Delta CT}$ method. The primer sequences were listed in Table 2.

Table 2: The real-time PCR primers

| <i>Gene</i> | | <i>Primer sequence</i> |
|-------------------|---------|------------------------|
| <i>AC083967.1</i> | Forward | TGTGACCTGATATCGGGGGT |
| <i>AC083967.1</i> | Reverse | CCCGACTGTGGCATCATCT |
| <i>AC106820.5</i> | Forward | GAGTTGTCAGGGAGGTTGGG |
| <i>AC106820.5</i> | Reverse | AGGGATGGGAGATGCTCACT |
| <i>AC245041.2</i> | Forward | TTGCTCAGACTGGACTGCAG |
| <i>AC245041.2</i> | Reverse | TATTTGGTGGGACCTTGGGC |
| <i>AL590617.2</i> | Forward | AGTGCTCAGTGTCACTCAGC |
| <i>AL590617.2</i> | Reverse | ACACATGCTGTCCCATCCAG |
| <i>AP002478.1</i> | Forward | AGGCAGCATACTGTGAACA |
| <i>AP002478.1</i> | Reverse | GCAGTGGAGGAATCACAGCT |
| <i>VPS9D1-AS1</i> | Forward | GAGGGACAAGAAGGCTGGTC |
| <i>VPS9D1-AS1</i> | Reverse | CAGCACGTCCTTGTCTCTGT |

Statistical analysis

The data analysis was conducted via R software (4.2.2) and GraphPad Prism (8.4.3). Student’s t-test and one-way ANOVA were employed to analyze the differences between two or more groups. $P < 0.05$ represents a significant difference.

Results

Determination of DRLs in HNSCC

In total, 16876 lncRNAs were collected from the HNSCC cohort. Then, the lncRNAs associated

with 23 DRGs were identified by correlation analysis (Fig. 2A). According to the criteria mentioned above, 292 DRLs were obtained, of which 290 DRLs had complete expression data (Table S2- not published). Of these 290 DRLs, a total of 24 DRLs were down-regulated and 266 DRLs up-regulated in the HNSCC. Further analysis revealed that only 161 DRLs were significantly different between HNSCC and normal tissues ($|\log_2(\text{fold change})| > 1$ and adjusted $P < 0.05$) (Fig. 2B).

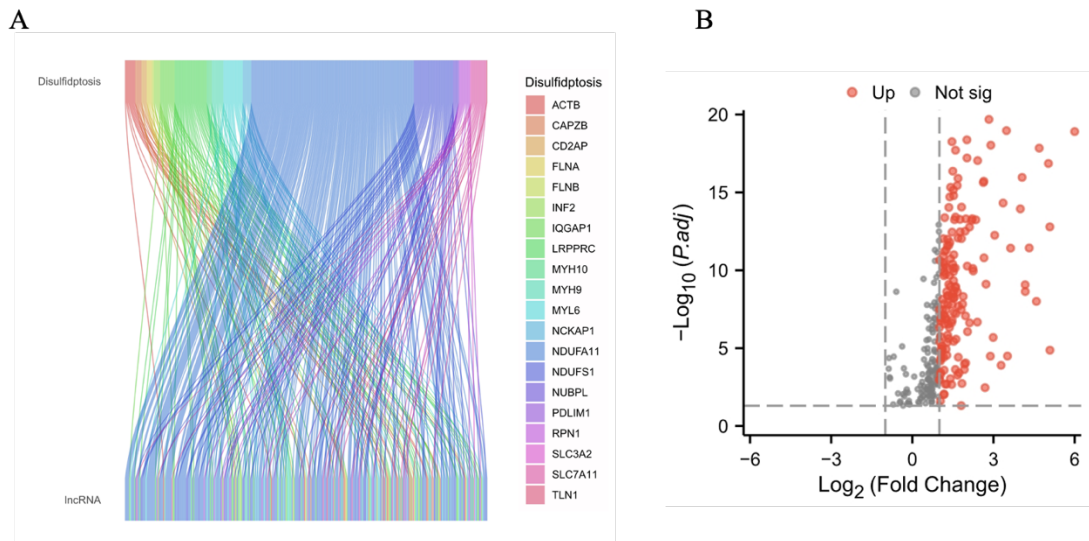


Fig.2: Disulfidptosis-related lncRNAs identification. A Correlation between disulfidptosis-related genes and associated lncRNAs. B Volcanic map of 290 disulfidptosis-related lncRNAs. Red points represent $\log_2(\text{fold change}) > 1$ and adjusted $P < 0.05$

Establishment and verification the DRLs risk model for HNSCC patients

Univariate COX regression showed that there were 26 DRLs significantly associated with the OS of HNSCC ($P < 0.05$) (Fig. 3A). Compared with non-tumor tissues, only SMILR was significantly down-regulated in HNSCC tissues ($P < 0.05$), while other 25 DRLs were significantly up-regulated ($P < 0.01$) (Fig. 3B and Table S2). To reduce the risk the over-fitting of the model, LASSO regression analysis was employed (Fig. 3C, D). Subsequently, we conducted multivariate

COX regression analysis and risk model coefficient analysis. Finally identified 6 DRLs used to construct the risk model, and the risk regression coefficient of each DRL was determined. The correlation between 6 DRLs and DRGs was shown in Fig. 3E. HNSCC patient's risk scores were calculated as follows: Risk Score = $AC106820.5$ expression $\times (-0.9854) + VPS9D1-AS1$ expression $\times 0.2134 + AL590617.2$ expression $\times 0.2751 + AP002478.1$ expression $\times 0.4996 + AC245041.2$ expression $\times 0.4419 + AC083967.1$ expression $\times 0.6881$.

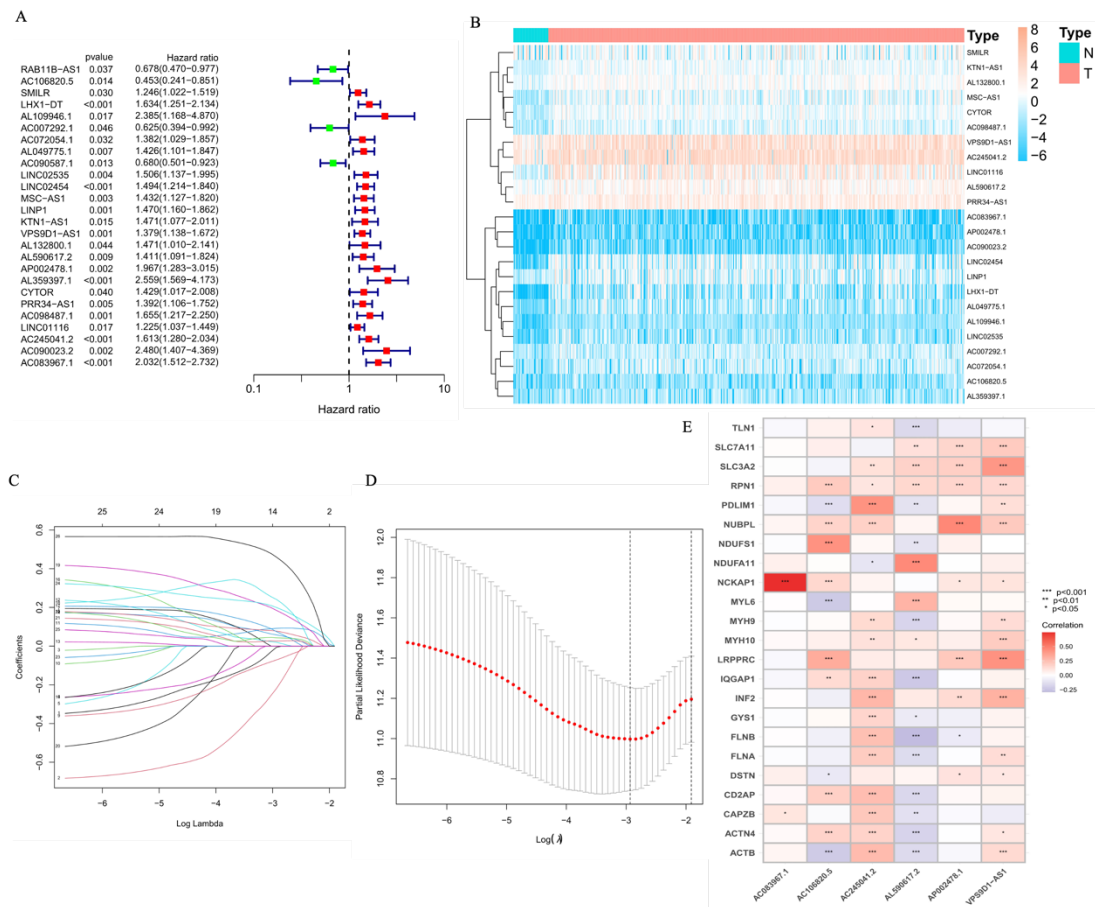


Fig. 3: Disulfidptosis-related lncRNAs prognostic model construction. A Univariate COX regression analysis of DRLs in HNSCC. B Heatmap for the prognostic lncRNAs in HNSCC. C The cross-validation for variable selection in LASSO model. D LASSO coefficient distribution. E The correlation of DRLs and disulfidptosis-related genes. * $P < 0.05$, ** $P < 0.01$, *** $P < 0.001$

The HNSCC patients with complete clinical information was randomly divided into a train group (N=256) and a test group (N=255). The

detailed clinical information of the two groups is shown in Table 1. There was no significant difference between the train and test groups

($P>0.05$), and the influence of artificial grouping difference on the results was excluded. Each patient's risk score was calculated and each group was divided into the high- and low-risk groups based on the median risk score value of the training group. The patients in each group were ranked according to the risk score (Fig. 4A-C). The patients in high-risk group had a higher mortality rate (Fig. 4D-F). Heatmaps displayed the expression of the 6 DRLs in each cohort (Fig.

4G-I), showing that only the expression of *AC106820.5* was decreased in the high-risk group, while the expression of other DRLs was increased. The survival analysis confirmed that the OS rate of the high-risk group was significantly lower than that of the low-risk group and the same result was also obtained in the testing group ($P<0.05$) (Fig. 4J-L), indicating that the DRLs prognostic model was successfully constructed.

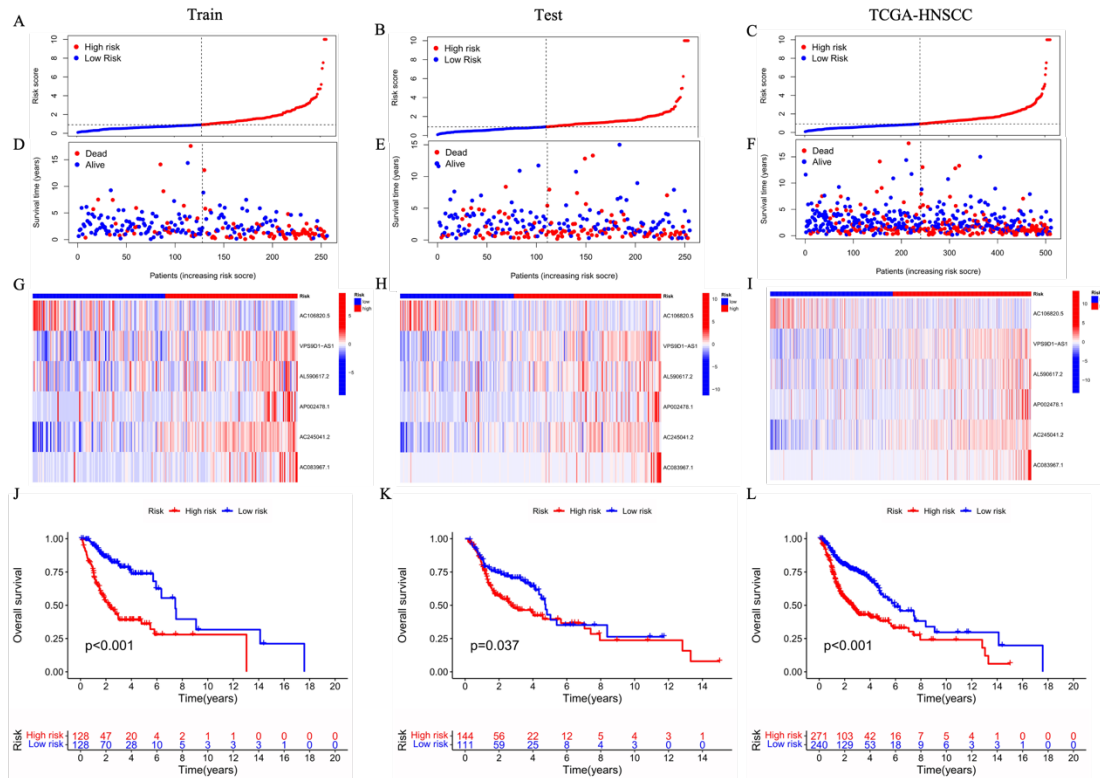


Fig. 4: Prognostic value of the 6 DRLs model. A-C Distribution of risk scores in the train, test, and TCGA-HNSCC cohorts. D-F Survival status in each group. G-I Heatmaps of the expression of DRLs in each group. J-L Kaplan–Meier curves of OS in each group

Relationships between DRLs prognostic model and clinical parameters

To further validate the superiority of the prognostic model, we first performed PCA using the 6 DRLs in the prognostic model and all DRLs, respectively. The results showed that compared with all DRLs, the difference between high- and low-risk patients was most significant in the prognostic model (Fig. 5A, B). We then grouped

all patients according to gender (female or male), age (≥ 60 or <60 yr), grade (G1-2 or G3-4), and stage (I-II or III-IV), and performed subgroup survival analyses. In each subgroup, patients in the high-risk group had lower OS than those in the low-risk group (Fig. 5C-J). In addition, we verified the predictive ability of the prognostic model by ROC curve. The areas under the curve (AUC) value at 1-, 3-, and 5-year were 0.641,

0.716, and 0.651, respectively (Fig. 5K). And the 3-year multifactor ROC curve result showed that the AUC value of the risk score was significantly higher than other clinical parameters (Fig. 5L).

The 6 DRLs prognostic model predicates the HNSCC patient's prognosis stably and effectively.

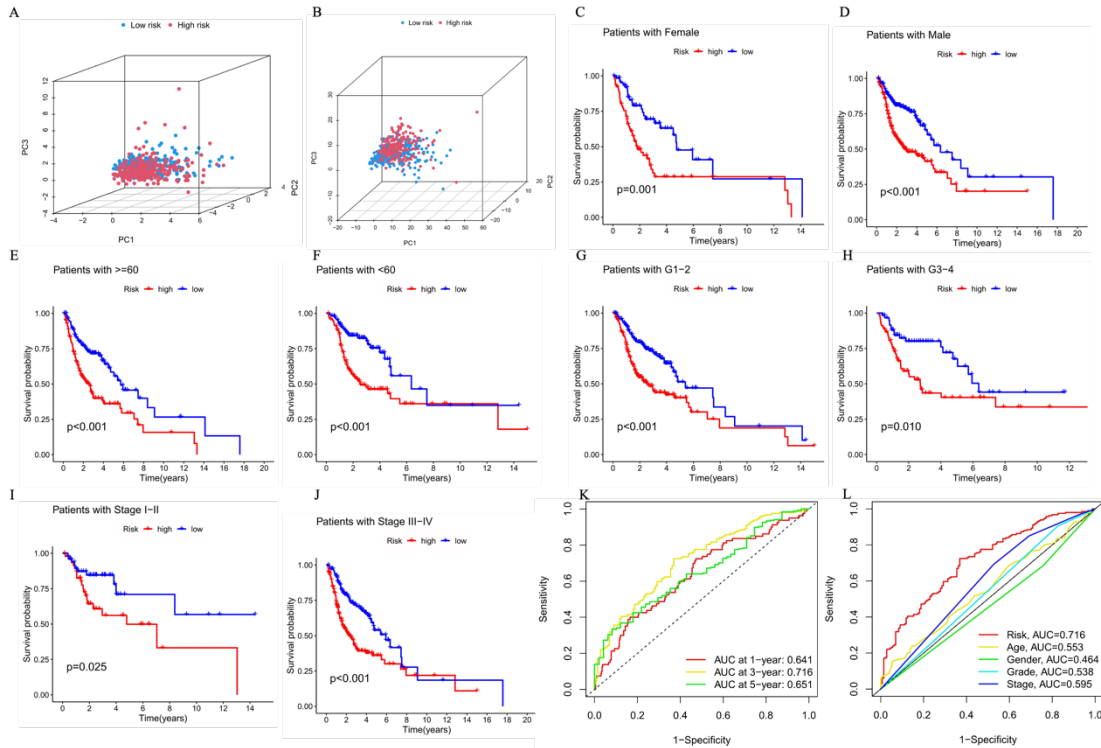


Fig. 5: Relationships between risk model and clinical parameters. A, B PCA based on the 6 risk DRLs and all DRLs, respectively. C-J OS curves for subgroups analysis. K ROC curves for 1-, 3-, and 5-year survival. L The 3-year ROC curves of risk score and clinical characteristics. * $P < 0.05$, ** $P < 0.01$, *** $P < 0.001$

Functional, GSEA and genetic variations in high- and low-risk groups

Overall, 588 genes were significantly differentially expressed between the high- and low-risk groups. The GO enrichment analysis showed that BP, CC, and MF mainly involved in antigen binding, immunoglobulin complex and immunoglobulin production respectively (Fig. 6A). Moreover, GSEA revealed that the top three enriched KEGG pathways in high-risk group were focal adhesion, Nod like receptor signaling pathway, and proteasome. While in the low-risk group, the top three enriched KEGG pathways were arachidonic acid metabolism, cell adhesion molecules

cams, and intestinal immune network for iga production (Fig. 6B). The 6 DRLs may be involved in immune regulation of HNSCC. Therefore, we used TIDE analysis to evaluate the ability of the prognostic model to predict immunotherapy effects, and the results showed that TIDE scores were elevated in the high-risk group, indicating an increased likelihood of immune escape in the high-risk group's patients (Fig. 6C) ($P < 0.05$). Finally, we examined somatic mutations in the high- and low-risk groups. The genes are most frequently mutated, with TP53 mutation rates ranking first in both groups and higher in the high-risk group (Fig. 6D, E).

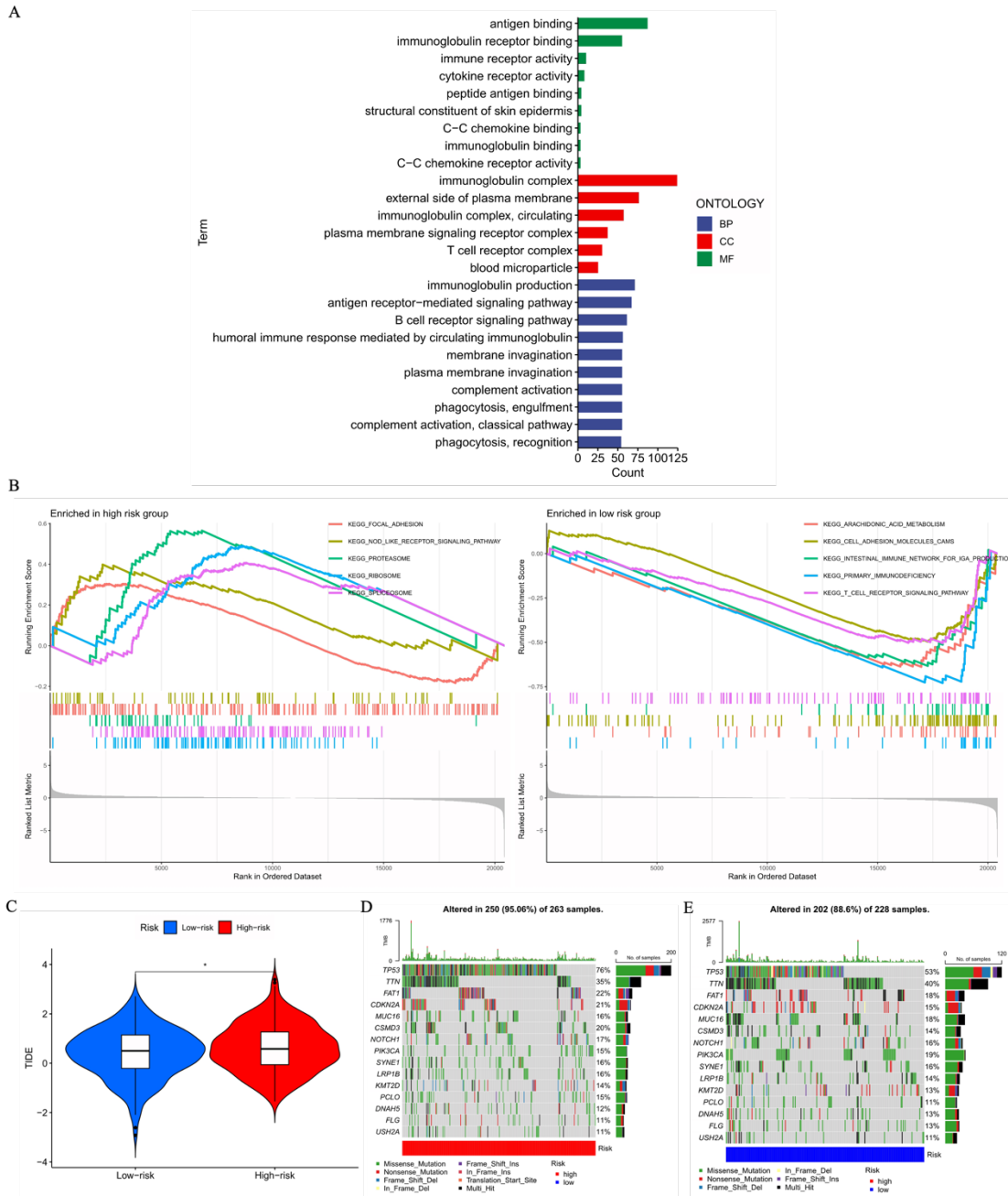


Fig. 6: Functional enrichment and somatic mutations analysis. A GO enrichment analysis. B GSEA of the top 5 pathways significantly enriched in the low- and high-risk groups. C TIDE analysis. D, E Oncoprint of the mutated genes in the low- and high-risk groups, respectively. * $P < 0.05$

Analysis of immunoinfiltration and chemotherapeutic drug therapy in prognostic model

We next found differences in immune cells between the high- and low-risk groups, the infiltration of B cell naïve, plasma cells, T cells regulatory cells, and mast cell resting cells were decreased,

while NK cells activated, macrophages M2, and mast cells activated were increased in low-risk group compared with the high-risk group (Fig. 7A, B). Meanwhile, there was significant difference in the almost all immune-related functions involved in analysis in different group (Fig. 7C).

Furthermore, immune score and ESTIMATE score were significantly lower in the high-risk group than in the low-risk group, suggesting a lower proportion of immune cells and a higher proportion of tumor cells in the high-risk group (Fig. 7D). In addition, we also conducted a drug sensitivity analysis, and the study results showed that VX-11e, dasatinib, SCH772984, and stauro-

sporine had potential effects on high-risk group (Fig. 7E-H). HNSCC patients at low-risk group showed increased sensitivity to apelisib, axitinib, oxaliplatin, and tamoxifen (Fig. 7I-L). Immune cell infiltration, immune function, and drug treatment effect were different significantly between two groups.

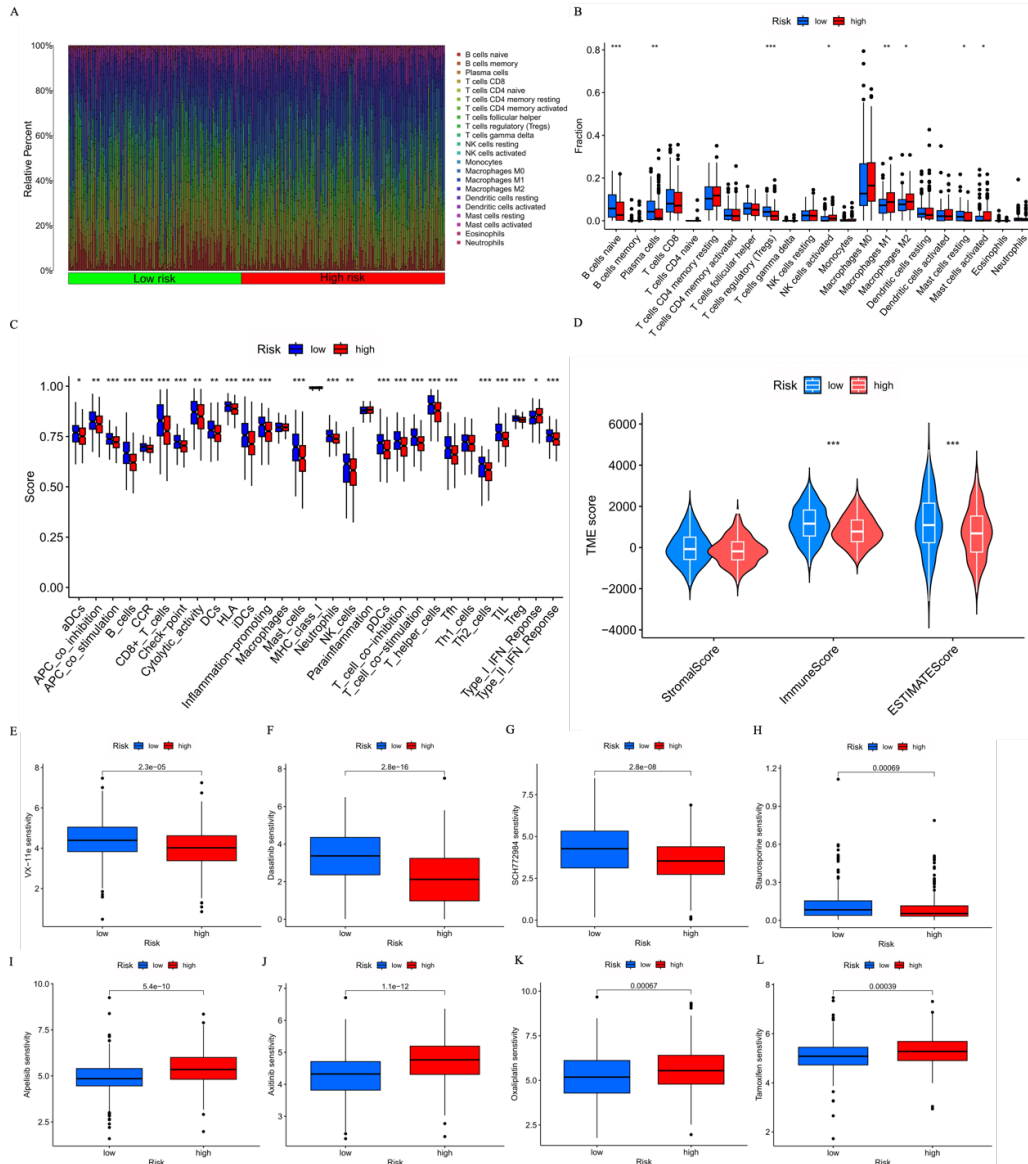


Fig.7: Tumor-infiltrating immune cells and drug sensitivity of the high- and low-risk groups. A Distribution of immune cells in the high- and low-risk groups. B A Box plot showing the immune cell infiltration in both groups. C Comparison of immune function between both groups. D Comparison of TIDE score between both groups. E-H Sensitive drugs for the high-risk group. I-L Sensitive drugs for the low-risk group

Validation of the RNA expression level of 6 DRLs in prognostic model

To analyze the expression level of the 6 DRLs, RT-PCR was conducted. As shown in Fig. 8, *AC083967.1*, *AC245041.2*, *AL590617.2*, *AP002478.1*, and *VPS9D1-AS1* were upregulated in the HNSCC cell lines (Fadu, WSU-HN6, and SCC-15) compared with those the human

normal oral keratinocyte epithelial cell line (HOK), while *AC106820.5* exhibited the down-regulated expression in the HNSCC cell lines than that in HOK. The expression of the 6 lncRNAs were consistent with the results of the model analysis, indicating that our previous bioinformatics analysis was accurate.

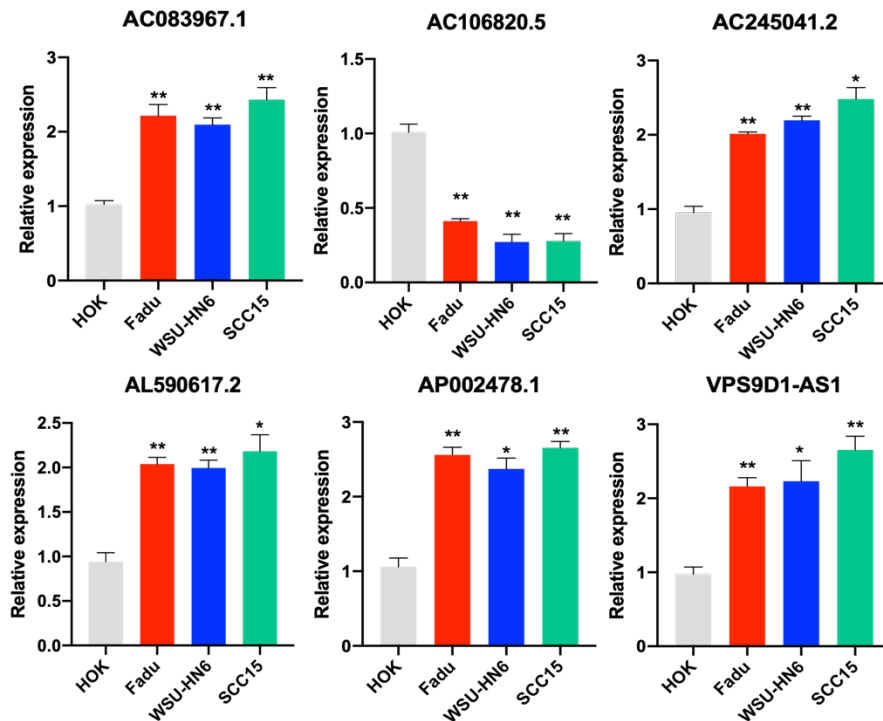


Fig. 8: Verification of the expression level of 6 DRLs in HNSCC cell lines by RT-PCR. * $P < 0.05$, ** $P < 0.01$

Discussion

An increasing number of researches has emphasized the prognostic values of DRLs in cancers (5-7). However, to our knowledge, there is currently no research on the correlation between DRLs prognostic model and HNSCC. Therefore, in this study, we constructed the DRLs prognostic model of HNSCC via bioinformatics methods for the first time. The accuracy of the novel model was evaluated via internal validation and in vitro experiments. The DRLs prognostic model could effectively predicate the prognosis and therapy response of HNSCC patients and is

meaningful to guide the personalize treatment plans and eventually improve the overall survival rate of HNSCC patients.

Different from the previously discovered mode of cell death, the mechanism by which disulfidptosis modulates tumor fate is not yet clear. So far, a limited number of DRGs has been identified. According to the previous studies, we choose 23 DRGs to obtain DRLs more relevant to the prognosis of cancers (5-8), and eventually 6 DRLs (*AC083967.1*, *AC106820.5*, *AC245041.2*, *AL590617.2*, *AP002478.1*, and *VPS9D1-AS1*) were identified. Notably, all the 6 DRLs were significantly related with the OS of

HNSCC patients in this research and had been proven to play functional roles in different tumor progression in previous researches (15-20). Accordingly, the 6 DRLs prognosis signature is highly likely to have good predictive value in HNSCC.

GO and GSEA analysis results showed that the DRLs prognosis signature was closely related to the immune regulation, which is consistent with the previous finding that disulfidptosis-related signature could characterize the immune micro-environment in cancer (21). Given the immune infiltration of TME is a determinate factor for the treatment efficacy of HNSCC patients (14), we further explored the relationship between the prognosis model and immune infiltration in more detail. There were more infiltration of anti-tumor cells infiltration including NK cells activated, macrophages M2, and mast cells activate compared with the high-risk group. TIDE analysis further confirmed the increased likelihood of immune escape in high-risk group's patients. Drug resistant is another key factor leading to the failure of HNSCC treatment. Therefore, potential targeted drugs for HNSCC were screened. Patients in different groups showed different drug sensitivity, suggesting that the novel DRLs signature could be an underlying index for evaluating the clinical therapy effects of HNSCC patients. Finally, we verified the 6 DRLs expression levels in the HNSCC cell lines, which was consistent with the bioinformatic analysis results. Accordingly, the 6 DRLs prognostic model could be served as a promising prognostic and therapeutic indicator for HNSCC.

Indeed, there were several limitations in the current study. For example, lack of more experimental validation. Therefore, further in vivo and in vitro investigations are worthy to conduct for the comprehensive understanding of the molecular mechanism of DRLs in the occurrence and development of HNSCC.

Conclusion

We successfully constructed the 6 DRLs signature with prognostic value in HNSCC. The DRLs

signature was associated with the tumor immune microenvironment, immunotherapy, and chemotherapy response. High-risk HNSCC patients are more likely to benefit from the immunotherapy and chemotherapy. There's a reasonable prospect that our research could provide valuable insight for clinical decision-making and personalized therapeutic of HNSCC.

Journalism Ethics considerations

Ethical issues (Including plagiarism, informed consent, misconduct, data fabrication and/or falsification, double publication and/or submission, redundancy, etc.) have been completely observed by the authors.

Acknowledgements

This work was supported by the Cultivating Project for Young Scholar at Hubei University of Medicine (Grant No: K1219601/2010QDJ19), the Humanities and Social Science Foundation, Hubei University of Medicine (Grant No: YHJ2020016).

Conflict of interests

The authors declare that they have no competing interests.

Data availability

This research followed the guidelines and policies for data access and publication specified by The Cancer Genome Atlas (TCGA) database (<https://portal.gdc.cancer.gov/>). Supplementary materials may be requested by respected readers from the corresponding author.

References

1. Sung H, Ferlay J, Siegel RL, et al (2021). Global Cancer Statistics 2020: GLOBOCAN Estimates of Incidence and Mortality Worldwide for 36 Cancers in 185 Countries.

- CA Cancer J Clin*, 71 (3): 209-49.
2. Johnson DE, Burtneß B, Leemans CR, et al (2020). Head and neck squamous cell carcinoma. *Nat Rev Dis Primers*, 6:92.
 3. Beltramini GA, Belloni LM, Fusco N, et al (2021). Comparing prognostic utility between the 8th edition of TNM staging system and the lymph node ratio for oral squamous cell carcinoma. *Head Neck*, 43 (10): 2876-82.
 4. Liu X, Nie L, Zhang Y, et al (2023). Actin cytoskeleton vulnerability to disulfide stress mediates disulfidptosis. *Nat Cell Biol*, 25: 404-14.
 5. Huang JQ, Zhang JY, Zhang FQ, et al (2023). Identification of a disulfidptosis-related genes signature for prognostic implication in lung adenocarcinoma. *Comput Biol Med*, 165:107402.
 6. Guo YW, Jiang ZP, Chen Q, et al (2023). Construction and experimental validation of a signature for predicting prognosis and immune infiltration analysis of glioma based on disulfidptosis-related lncRNAs. *Front Immunol*, 14:1291385.
 7. Xu KQ, Dai CX, Yang JL, et al (2024). Disulfidptosis-related lncRNA signatures assess immune microenvironment and drug sensitivity in hepatocellular carcinoma. *Comput Biol Med*, 169:107930.
 8. Kang K, Li XX, Peng YH, et al (2023). Comprehensive Analysis of Disulfidptosis-Related lncRNAs in Molecular Classification, Immune Microenvironment Characterization and Prognosis of Gastric Cancer. *Biomedicines*, 11(12):3165.
 9. Savic D, Steinbichler TB, Ingruber J, et al (2023). Erk1/2-Dependent HNSCC Cell Susceptibility to Erastin-Induced Ferroptosis. *Cells*, 12 (2): 336.
 10. Sandulache VC, Ow TJ, Pickering CR, et al (2011). Glucose, not glutamine, is the dominant energy source required for proliferation and survival of head and neck squamous carcinoma cells. *Cancer*, 117 (13): 2926-38.
 11. Kung JT, Colognori D, Lee JT (2013). Long noncoding RNAs: past, present, and future. *Genetics*, 193 (3): 651-69.
 12. Ma H, Chang H, Yang W, et al (2020). A novel IFNalpha-induced long noncoding RNA negatively regulates immunosuppression by interrupting H3K27 acetylation in head and neck squamous cell carcinoma. *Mol Cancer*, 19:4.
 13. Li H, Xiong HG, Xiao Y, et al (2020). Long Non-coding RNA LINC02195 as a Regulator of MHC I Molecules and Favorable Prognostic Marker for Head and Neck Squamous Cell Carcinoma. *Front Oncol*, 10: 615.
 14. Zou W (2022). Immune regulation in the tumor microenvironment and its relevance in cancer therapy. *Cell Mol Immunol*, 19: 1-2.
 15. Liu S, Zhang S, Liu Y, Yang X, Zheng G (2023). Comprehensive analysis of cuproptosis-related long noncoding RNA for predicting prognostic and diagnostic value and immune landscape in colorectal adenocarcinoma. *Hum Genomics*, 17: 22.
 16. Wang E, Li Y, Ming R, et al (2021). The Prognostic Value and Immune Landscapes of a m(6)A/m(5)C/m(1)A-Related lncRNAs Signature in Head and Neck Squamous Cell Carcinoma. *Front Cell Dev Biol*, 9: 718974.
 17. Wei J, Zeng Y, Gao X, Liu T (2021). A novel ferroptosis-related lncRNA signature for prognosis prediction in gastric cancer. *BMC Cancer*, 21: 1221.
 18. Feng L, Yang K, Kuang Q, Peng M, Li L, Luo P (2022). A Novel Risk Model for lncRNAs Associated with Oxidative Stress Predicts Prognosis of Bladder Cancer. *J Oncol*, 2022: 8408328.
 19. Liu YY, Zhu JY, Ma XL, et al (2019). ceRNA network construction and comparison of gastric cancer with or without Helicobacter pylori infection. *J Cell Physiol*, 234 (5): 7128-40.
 20. Yang L, Dong X, Liu Z, et al (2022). VPS9D1-AS1 overexpression amplifies intratumoral TGF-beta signaling and promotes tumor cell escape from CD8(+) T cell killing in colorectal cancer. *Elife*, 11: e79811.
 21. Tang J, Peng X, Xiao D, et al (2024). Disulfidptosis-related signature predicts prognosis and characterizes the immune microenvironment in hepatocellular carcinoma. *Cancer Cell Int*, 24(1):19.